Scanning tunnelling spectroscopy of atomic clusters deposited on oxidized silicon surfaces: induced surface dipole and resonant electron injection

2003 J. Phys.: Condens. Matter 15 S3065

(http://iopscience.iop.org/0953-8984/15/42/006)

INSTITUTE OF PHYSICS PUBLISHING JOURNAL OF PHYSICS: CONDENSED MATTER

J. Phys.: Condens. Matter **15** (2003) S3065–S3081 PII: S0953-8984(03)64929-5

Scanning tunnelling spectroscopy of atomic clusters deposited on oxidized silicon surfaces: induced surface dipole and resonant electron injection

Leonid Bolotov[1], **Noriyuki Uchida and Toshihiko Kanayama**

Advanced Semiconductor Research Centre, National Institute of Advanced Industrial Science and Technology, 1-1-1 Higashi, Tsukuba, Ibaraki 305-8562, Japan

E-mail: bolotov.leonid@aist.go.jp

Received 17 June 2003, in final form 15 August 2003
Published 10 October 2003
Online at stacks.iop.org/JPhysCM/15/S3065

Abstract

We investigated the tunnelling conductance of atomic clusters (C_{60}, Si_6H_x, $AsSi_2H_x$) deposited on oxidized p-type Si(100) surfaces using scanning tunnelling microscopy where the metal probe/vacuum barrier/cluster/oxide/silicon structures form an asymmetric double-barrier tunnel (ADBT) nanoscale junction. Atomic clusters were assembled onto ultra-thin (∼0.3 nm) silicon oxide by either C_{60} sublimation or ion beam deposition of Si-clusters generated in an ion trap. Electron transfer to the clusters induced surface dipole and reduced junction current under reverse biasing conditions (negatively biased substrate) depending on cluster structure and composition, where the $AsSi_2H_x$ clusters created the strongest dipole. Conductance enhancement was observed for forward bias originating in resonance-like electron injection through the unoccupied orbital of the clusters, which was spatially localized within ∼1 nm diameter for C_{60}. The resonance peak positions and the weak surface dipole indicated that the orbital energies of C_{60} and Si_6H_x were beyond the forbidden energy gap of Si and shifted with respect to the silicon Fermi energy for heavily doped substrates. In contrast, the orbital energy of doped $AsSi_2H_x$ clusters was below the silicon Fermi level. These results demonstrate that the ADBT junction configuration reveals electronic coupling of the clusters to the semiconductor surfaces.

1. Introduction

Electronic devices made of silicon are becoming progressively smaller. As device structures continue to shrink, the ability to control carrier transport is becoming less straightforward

[1] Author to whom any correspondence should be addressed.

because tiny changes in structures and quantum effects such as tunnelling considerably influence their performance. One possible way to achieve atomic-scale control over carrier transport is to introduce molecules and atomic clusters into the active regions of devices. For example, it has been observed that current–voltage characteristics become non-monotonic and sometimes exhibit negative differential resistance (NDR) in Schottky diodes with an organic functional interlayer (Li *et al* 1988), and metal/molecular film/metal junctions (Reed *et al* 1997, Chen *et al* 2000, Amlani *et al* 2002). These unique features introduced by atomic clusters and molecules enable desirable operations in devices such as organic light emission diodes, organic thin-film transistors and molecular switches (Aviram and Ratner 1974), thus stimulating extensive research in this area (Dujardin *et al* 1992, Tans *et al* 1998, Gimzewski and Joachim 1999, Hersam *et al* 2000, Donhauser *et al* 2001).

Since tunnelling phenomena by electrons penetrating through narrow potential barriers were discovered, these have been utilized in various forms for device operations. Resonant tunnelling, for instance, was applied to semiconductor heterostructure tunnel devices, where tunnel current is enhanced at the energy of a localized state within the tunnelling barrier (Wolf 1985, Kelly 1995, Liu *et al* 1991, Shen *et al* 1995, Suda and Koyama 2001). Such enhanced tunnelling is well known in the resonant-tunnelling spectroscopy of field-emission electrons for atoms adsorbed on metal surfaces (Gadzuk 1970, Persson and Baratoff 1987, Gata and Antoniewicz 1993). Particularly interesting here is tunnelling spectroscopy that uses resonance excitation of adsorbed molecules. Conductance measurements of molecules have been performed in various mesoscopic tunnel junction geometries to identify their electron and phonon spectra. Mazur and Hipps examined resonance-like conductance via the lowest unoccupied molecular orbital (LUMO) for a list of molecules introduced into Al–AlO_x–molecule–Pb junctions where electrons were injected from Al electrodes (Mazur and Hipps 1994a). When a self-assembled monolayer (SAM) of organic molecules (sulfur-tailed molecules on Au) was placed between two metal electrodes, junction conductance was found to depend on the internal structure of the molecule (Reed *et al* 1997, Chen *et al* 2000). This demonstrates that tunnelling spectroscopy is an important method in the study of molecules and atomic clusters on solid surfaces.

When a cluster/molecule is placed on a metal surface, its molecular levels line up with respect to the metal Fermi energy. Xue and Datta (1999) theoretically investigated the line-up problem in single-wall carbon nanotubes supported on a gold substrate as a function of nanotube–surface separation. They obtained an orbital energy of $\sim$0.2 eV above the metal Fermi energy for 1.5 nm separation and $\sim$0.5 eV for 0.5 nm, where the shift was caused by local electrostatic potential perturbation of the orbital due to charge transfer (Xue and Datta 1999). Moreover, effects of the local environment and electronic couplings within and between molecules and interfaces were observed for individual alkyl molecules where molecule appearance changed over time upon molecule conformations (Bumm *et al* 1999, Donhauser *et al* 2001, Roland *et al* 2002).

Alignment of cluster levels at the semiconductor surface seems similar to the band line-up in semiconductor hetero-junctions where the band line-up is derived from overlap between the tail of the wavefunction of a semiconductor decaying into another while maintaining local charge neutrality (Capasso and Margaritondo 1987, Margaritondo 1999). In contrast, alignment of localized cluster levels is not obvious because it may trap charge and form a surface dipole that modifies intrinsic distributions of mobile carriers (electrons and holes) at the surface, and consequently, alignment. Furthermore, dangling bonds of surface atoms on bare semiconductor surfaces make covalent bonds with a molecule, changing internal electronic structures both in the molecule and the surface and resulting in bias-polarity dependent current and diode-like rectification. This was observed in scanning tunnelling microscopy (STM)

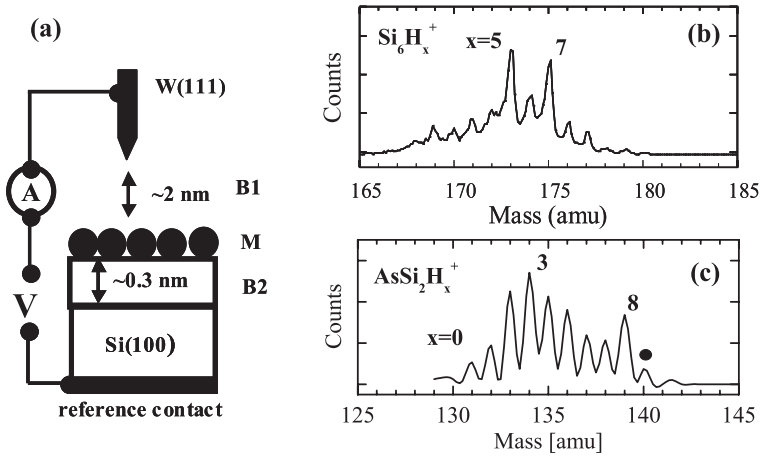

Figure 1. (a) Junction structure: B1—vacuum gap barrier, M—cluster layer, B2—ultra-thin oxide spacer. Voltage supplier (V) and tunnelling current meter (A) are shown. High-resolution mass spectra of cluster ion beams containing Si_6H_x (b) and $AsSi_2H_x$ (c) clusters. Numbers are x values. Peak ● is due to the silicon isotope.

measurements at the nickel phthalocyanine (Ni-Pc) overlayer on Si(111)-(7×7) surfaces where the geometrical asymmetry of a junction containing molecular state resonance determined current behaviour (Ottaviano *et al* 1997).

In this study, we investigated the current–voltage characteristics of metal probe/insulator (vacuum)/cluster/oxide/silicon (MICOS) structures containing different types of atomic cluster (C_{60}, Si_6H_x, $AsSi_2H_x$) to elucidate cluster–substrate interaction and resonant tunnelling mediated by the cluster orbital. The MICOS structures form an asymmetric double-barrier tunnel (ADBT) junction (figure 1) where the STM probe tip works as a metal electrode separated by a vacuum barrier from the Si(100) surface, and atomic clusters placed within the barrier are separated from the Si substrate by a well defined, ultra-thin oxide spacer. The oxide spacer prevents chemical bonding of clusters to dangling bonds of surface Si atoms and, consequently, reduces coupling to the substrate. Since single-electron tunnelling (SET) effects are often observed in such double-barrier junctions, the flexibility of the STM vacuum barrier was used to adjust electron injection rate to assess the alignment of the cluster orbital on silicon surfaces. Such a double-barrier junction geometry has previously been used to investigate the interplay between molecular states and SET effects in C_{60} on gold films, where a large barrier between C_{60} and gold film was uncontrollably formed with amorphous carbon and hydrocarbons (Porath and Millo 1997). Similar junction configurations were recently used for fluorescence excitation in porphyrin molecules at a thin Al_2O_3/NiAl(110) surface with submolecular precision by electron injection into the LUMO + 1 orbital from STM probes (Qiu *et al* 2003).

In this paper, we first outline the experimental procedure to prepare the substrate and deposit the clusters for scanning tunnelling spectroscopy (STS) measurements (section 2). Section 3 discusses diode-like behaviours of the junction containing the clusters in terms of asymmetric carrier transport through the junction under different electron injection conditions. An effective cluster charge (surface dipole) that reflects the strength of cluster coupling to the underlying Si is evaluated (section 3.3) for different cluster types and densities. Section 4 presents analysis of the conductance spectra and $(\mathrm{d}I/\mathrm{d}V)$ maps for C_{60} and Si_6H_x clusters to assess electron injection from the metal STM probe, where cluster-specific enhancement

of the conductance originates in resonance-like electron injection through the cluster orbital located above the conduction band edge of Si. Finally, we discuss the alignment of the cluster orbital with respect to silicon Fermi energy considering energy shift and broadening of the C_{60} orbital for highly doped substrates.

2. Cluster deposition

Substrates for cluster deposition were prepared from p-type (boron-doped, 0.01–10 Ω cm) Si(100) wafers. An atomically flat Si(100)-(2 × 1) surface was formed by flash-heating samples to 1100 °C for ∼20 s in an ultra-high vacuum (UHV) of $\sim 4 \times 10^{-9}$ Pa. Oxide growth was performed by exposing Si(100)-(2 × 1) surfaces to ∼1000 L (Langmuir) molecular oxygen at a pressure of $\sim 10^{-5}$ Torr and room temperature (RT) followed by annealing at 400 °C. Monomolecular films of C_{60} were obtained by vapour deposition of C_{60} at RT followed by short annealing at 150–170 °C; details of this technique have been described elsewhere by Bolotov and Kanayama (2002). One side of the wafer was doped to a high level with boron with a conventional ion implantation technique for electrical measurements.

Si_6H_x and $AsSi_2H_x$ clusters were deposited by exposing the oxidized surface to a cluster ion beam extracted from an external quadrupole static attraction ion trap (EQSIT) at RT (Kanayama 1994, Uchida *et al* 2003b, Hiura *et al* 2001). A high-resolution mass spectrum of the Si_6H_x ion beam (see figure 1(b)) revealed that the dominant component of clusters had $x = 5$ (∼43%), 7 (∼23%) and 3 (∼15%). Arsenic-doped Si clusters were generated by introducing ionized arsine into the EQSIT chamber in addition to silane gas. The resulting ion beam contained $AsSi_2H_x$ clusters of $x \leqslant 8$ as seen in figure 1(c) with a content of ∼60% and a small amount of hydrogenated Si_5 and Si_4. An impact kinetic energy below 18 eV was chosen, ensuring soft landing of the Si_6H_x clusters (Uchida *et al* 2003a). The cluster density was estimated from both STM topographs and exposure dose, and the maximum density was about 10^{12} cm^{-2}.

Tunnelling conductance measurements were made with a UHV Omicron SPM set-up operating at RT. STM probe tips were prepared from a single-crystalline W(111) wire and cleaned *in situ* with field-emission microscopy. Current–voltage (I–V) characteristics were obtained by opening the current feed-back loop and ramping sample voltage while measuring tunnelling current. The initial tunnelling conditions were set by tunnelling current and applied bias voltage, hereafter called the onset current and the onset voltage. Their ratio is called the onset conductance G_o. The probe–substrate distance (junction width) was regulated by controlling the onset tunnelling current in a range of 0.1–50 nA and at an onset voltage of 1.2–2.5 V corresponding to electron injection from the probe tip into the substrate. STM constant-current topographs and conductance maps were obtained keeping the feed-back loop closed (constant-current mode). We made the measurements under dark conditions protecting the sample against any illumination. Conductance spectra were calculated from I–V characteristics averaged for 10–200 different clusters to compensate for the effects of local variations and cluster conformations.

Exposure of Si(100)-(2 × 1) surfaces to molecular oxygen left a flat surface without any ordered structure as seen in figure 2(a), where atomic steps run from the bottom left to the top right corner. The step height was 0.24–0.27 nm and equal to that of the initial Si(100)-(2 × 1) surface. We infer that the oxide thickness was ∼0.3 nm according to reports on oxidation under similar conditions. In these, a thickness of about 0.3 nm has been reported for oxides thermally grown on Si(100)-(2 × 1) surfaces under oxygen pressures of 10^{-6}–10^{-5} Torr at 470–725°C for less than 10 min, which was determined by x-ray photoelectron spectroscopy (Miyata *et al* 1999) and scanning reflection electron microscopy (SREM) during oxide growth

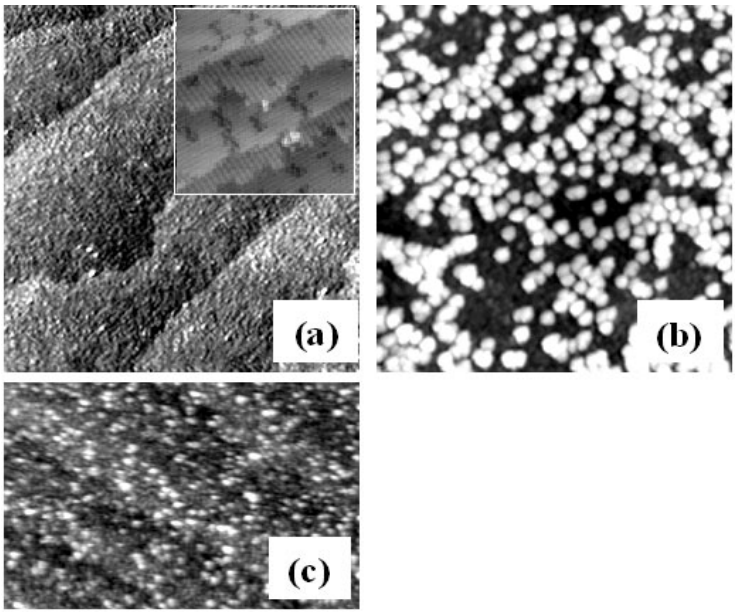

Figure 2. STM topographs of ∼0.3 nm oxidized Si(100)-(2 × 1) surfaces before (a) and after deposition of C_{60} (b) and Si_6H_x (c) clusters. Cluster density was $\sim 3 \times 10^{12}$ cm^{-2} in (c) and $\sim 2 \times 10^{13}$ cm^{-2} in (b). Image areas are 50 × 50 nm^2 in (a) and (b), and 50 × 30 nm^2 in (c). The inset in (a) shows a 20 × 20 nm^2 area of Si(100)-(2 × 1) surface prepared after flash-heating at 1100 °C. Onset voltage was +2 V and tunnelling current was 0.3 nA.

(Fujita *et al* 1997). The SREM observations also demonstrated the presence of an atomically flat interface where the two topmost layers of Si atoms on the Si(100)-(2 × 1) surface were oxidized.

Cluster deposition changed the surface morphology. For example, at low density, Si_6H_x clusters appeared as bright protrusions (figure 2(c)) with apparent heights distributed around ∼0.4 and ∼0.6 nm. These values were in good agreement with the calculated diameters of an Si network for Si_6 (0.41 nm) and Si_6H_7 (0.38 nm) corresponding to compact cluster structures (Uchida *et al* 2003b, Miyazaki *et al* 1996). This indicates that most clusters maintain their structures after landing on the surface. This was confirmed in separate experiments on Si(111)-(7 × 7) surfaces where the fragmentation of Si_6H_x occurred at a cluster kinetic energy above ∼3 eV/Si atom (Uchida *et al* 2003a). The clusters larger in height were tentatively ascribed to those adsorbed at positions that were slightly distant from the Si surface due to thickness variation of the oxide layer.

With increased cluster density, the atomic steps in figure 2(a) disappeared and the surface roughness increased ∼4-fold (rms ∼ 0.35 nm) for C_{60} and ∼2-fold for Si clusters in comparison to that of the oxidized surface (rms ∼ 0.08 nm), providing evidence of cluster film formation. The apparent height of isolated C_{60} clusters observed in empty-state STM topographs was approximately equal to those measured on metal and silicon surfaces (Sakurai *et al* 1996), suggesting sufficient transparency in the oxide barrier for STM/STS measurements.

The clusters were relatively immobile on the oxidized surfaces as was observed during continuous imaging of cluster films for an hour. The fraction of relocated clusters was about 5–10% for C_{60} and Si_6H_x, but the majority of the clusters was stationary, allowing conductance measurements.

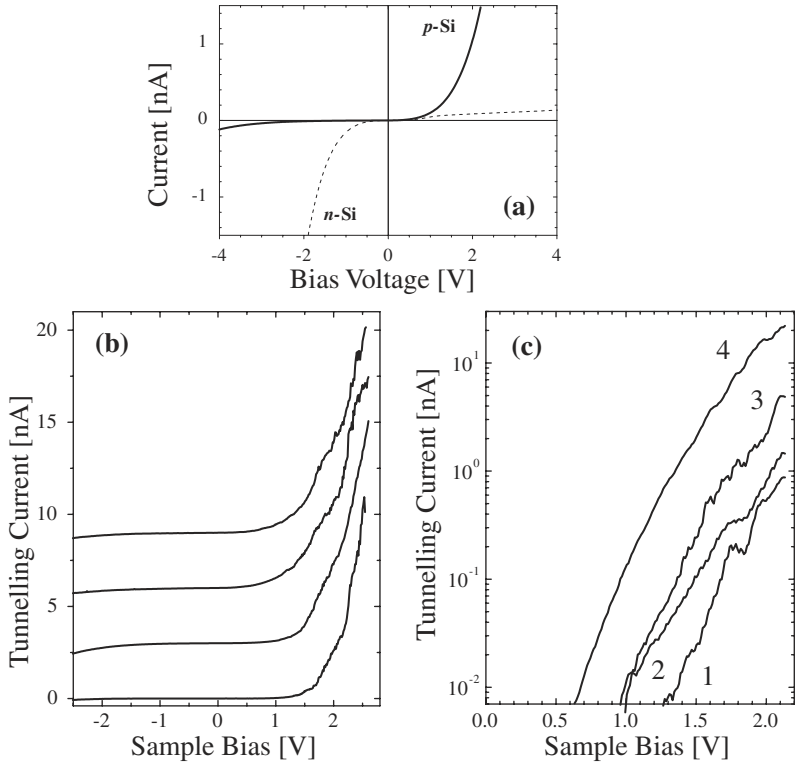

Figure 3. (a) Diode-like current–voltage characteristics of STM junction at oxidized Si(100)-(2 × 1) surfaces without clusters: p-Si, boron, $\sim 4 \times 10^{15}$ cm^{-3} (solid curve) and n-Si, antimony, $\sim 8 \times 10^{14}$ cm^{-3} (broken curve). Onset tunnelling current is 1 nA, and onset bias voltage is +2 V and −1.8 V for p-Si and n-Si, respectively. (b) Average tunnelling current of STM junction containing C_{60} obtained in different locations at +2 V and 2 nA. Current asymmetry is clearly seen. Curves have been shifted upward for the sake of clarity. (c) Forward current of STM junction containing Si_6H_x clusters as a function of sample bias voltage for different vacuum gap barriers. Curves 1–4 correspond to onset tunnelling currents of 0.56 nA (1), 0.85 nA (2), 2.0 nA (3) and 16.0 nA (4) at onset voltage of +2 V.

3. STM diode characteristics

3.1. Oxidized Si(100) surfaces

Current–voltage characteristics of the junction, both with and without clusters, were asymmetric (figure 3(a)). The current increased exponentially with positive bias voltage for p-Si substrates, while little change in tunnelling current was observed at negative bias. Conversely, opposite current asymmetry in *I–V* characteristics was observed for n-Si substrates oxidized under the same conditions. Such asymmetry in STM current characteristics occurred on low-doped Si surfaces after hydrogenation or oxidation (Kaiser *et al* 1988, Tabe and Tanimoto 1991, Bolotov *et al* 1995), and on cleaved GaAs surfaces (Feenstra *et al* 1993). These researchers discussed current behaviour in terms of metal–insulator–semiconductor (MIS) tunnel diode operation where current asymmetry originates in bias-dependent distribution of applied voltage between the tunnelling junction and the depletion region beneath the probe electrode. Under forward biasing of p-Si (positive bias voltage) majority carriers (holes) are attracted to the tunnelling junction, reducing the depletion region. In contrast, at reverse

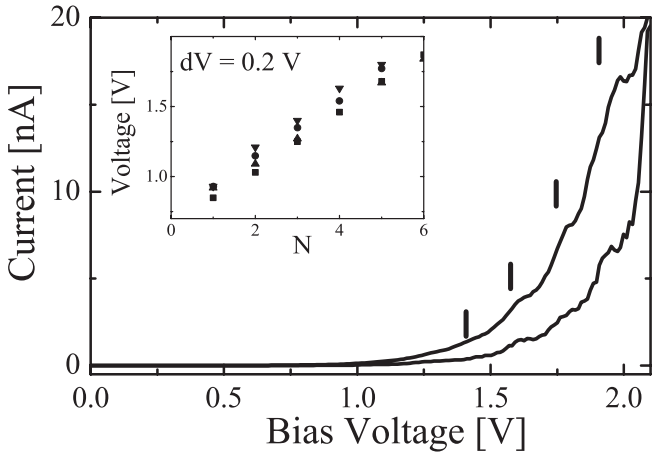

Figure 4. Forward current of STM junction containing Si_6H_x clusters with apparent heights of ∼0.7 nm at onset conductance of 3.3 and 8 nS (upper curve). The inset shows step voltage for four clusters; step separation is ∼0.2 V.

bias the electric field repels holes expanding the depletion region, while it drives electrons (minority carriers) to the junction, where they tunnel into the probe electrode. In our substrates, the density of minority carriers was negligibly small with respect to the density of majority carriers, thus leading to a current asymmetry that was typical for planar MIS tunnel diodes (Green *et al* 1974).

In the MIS diode picture, the presence of surface states within the energy bandgap and static charges substantially influences the I–V characteristics of the junction. In fact, only when Si dangling bonds were terminated by hydrogenation or oxidation were diode-like characteristics of STM junctions observed (Kaiser *et al* 1988, Tabe and Tanimoto 1991, Bolotov *et al* 1995). Conventional furnace oxidation produces a gap-state density of about 10^{10} cm^{-2} for Si(100) and less than 10^{12} cm^{-2} for Si(111) surfaces (Sze 1981). Low-pressure oxidation below 600 °C also results in a density of $\sim 10^{12}$ cm^{-2} for Si(100) surfaces (Bitzer *et al* 2000, Miyata and Ichikawa 2001). A similar gap-state density of about 10^{11} cm^{-2} was obtained for C_{60}/H:Si heterojunctions, indicating that C_{60} did not create interface defects (Kita *et al* 1997). We found that the tunnelling current lost its diode-like behaviour and significantly increased at reverse bias over surface defects that had energy states within the Si forbidden gap. We estimated gap-state density by counting high-current sites and obtained a residual density of gap states of (3–8) $\times$ 10^{11} cm^{-2} for which I–V characteristics were measured over a wide area with ∼1 nm spacing. A gap state density of $\sim 2 \times 10^{12}$ cm^{-2} was found for an Si(100)-(2 $\times$ 1) surface after atomic hydrogen exposure with ∼200 L. Both the diode-like behaviour and the low residual density of gap states indicate that our oxidation conditions leave the low gap-state density required for weak cluster–substrate coupling.

3.2. Cluster deposited surfaces

Cluster deposition modified the current–voltage dependence of tunnel junctions. The most prominent change was observed at forward bias where the current increased non-monotonically with bias voltage. Figure 3(b) shows STM I–V characteristics of C_{60} averaged over ∼20 clusters in different places on the surface, where broad features reproducibly appeared at ∼1.5 and 2.3 V, while no structure was observed at negative bias voltage. Forward current exhibited

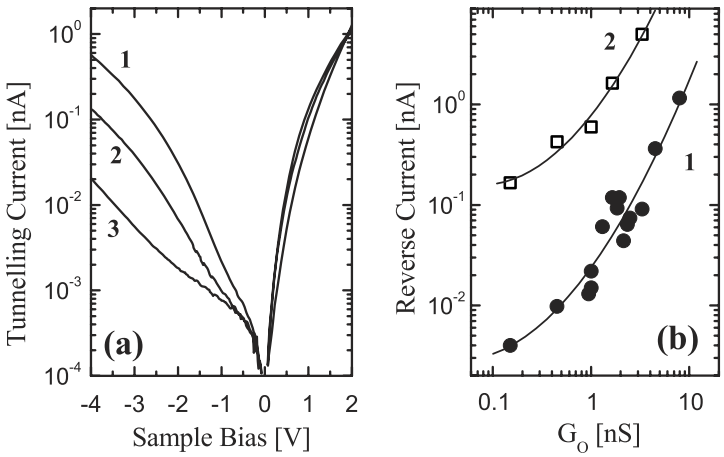

Figure 5. (a) Area-averaged I–V characteristics of STM junction at oxidized surface of Si(100) (boron, $\sim 2 \times 10^{15}$ cm^{-3}) subjected to $AsSi_2H_x$ ($x \leqslant 8$) cluster beams as a sequence of exposures at ∼5 pA for 2 h (1), ∼7 pA for 2 h (2) and ∼3 pA for 2 h (3). Maximum cluster density is $\sim 8 \times 10^{11}$ cm^{-2}. Onset voltage is +1.8 V and onset current is 1.0 nA. (b) Reverse current at −3 V as a function of onset forward conductance G_o at +1.8 V for a junction containing $AsSi_2H_x$ clusters (●). Data for the oxidized surface (□) were obtained on the same sample outside the deposited area. Curves are best fits to functions of $\sim(G_o^2 + 2.7G_o)$ for clusters and $\sim(G_o^2 + 2.3G_o)$ for oxide.

an NDR feature at ∼1.7 V for Si_6H_x clusters (figure 3(c)) when the onset current was about 0.1–10 nA, while it disappeared when the current was increased by bringing the probe tip closer to the surface. At high current injection, significant direct current into the Si band took over cluster-related current, resulting in structureless characteristics.

A small fraction (∼10%) of Si_6H_x clusters that had an apparent height of ∼0.7 nm exhibited periodic current steps of ∼0.2 V (figure 4). Periodic current steps of ∼0.4 eV have previously been observed for C_{60}/hydrocarbon/gold surfaces as a result of a SET behaviour (Porath and Millo 1997). When a cluster is distant from the Si surface, it stores injected electrons for a longer time than the interval between tunnelling of individual electrons, leading to Coulomb interaction between the stored and tunnelling electrons. When the vacuum barrier is very small, resulting in high onset current, SET effects may appear, although the Coulomb energy of ∼0.2 eV obtained here is too small for a cluster diameter of ∼0.4 nm, and also the number of stored electrons, i.e. the number of current steps (four to six), is too large to maintain cluster integrity. Taking this into account, we restricted the injection rate to a tunnelling current of 10 nA and a conductance G_o of 3 nS in our experiments to prevent such effects from appearing.

3.3. Cluster-induced dipole

Cluster deposition resulted in a reduction of STM reverse current for low-doped p-Si substrates. Figure 5(a) shows STM I–V characteristics after repeatedly exposing the oxidized surface to $AsSi_2H_x$ ($x \leqslant 8$). Because of their small size and low density on the disordered oxidized Si(100) surface, cluster recognition from STM topographs was difficult. Thus I–V characteristics were acquired over 200×200 nm^2 areas with 1–5 nm spacing. We see that reverse current is reduced by an order of magnitude as cluster density increases, while forward current is essentially the same. Reverse current remained the same after cluster exposure on a part of the sample surface where no clusters had been deposited.

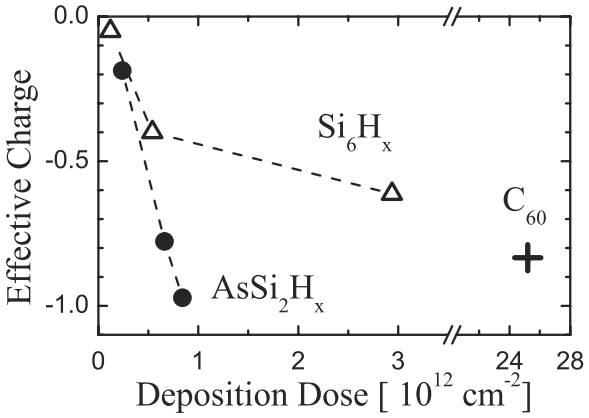

Figure 6. Effective cluster-induced charge at oxidized Si surface for $AsSi_2H_x$ clusters (●) and Si_6H_x clusters (△) calculated from STM reverse currents (see text). The cross shows effective charge for C_{60} at a density of $\sim 2 \times 10^{13}$ cm^{-2}.

There are two factors that determine reverse current value: the effective tunnelling barrier and the density of electrons (minority carriers) available for tunnelling at the Si surface. The fact that forward current remained unchanged after cluster deposition (figure 5(a)) indicates the weak influence of the clusters on the effective tunnelling barrier. To confirm what influence the effective barrier had, we decreased the vacuum barrier width by bringing the probe tip closer to the surface, resulting in increased forward conductance G_o. The dependence of reverse current on G_o is shown in figure 5(b) for the junction formed before and after cluster deposition. We obtained similar functional dependence, while the current value was lowered after deposition. This ruled out change in the effective tunnelling barrier as a dominant factor to reduce reverse current. Consequently, carrier distribution at the Si surface changes due to the clusters.

When clusters create an electrostatic surface dipole, electron density at the Si surface changes in accordance with the charge transferred onto the cluster. Positively charged clusters produce an attracting force for electrons; otherwise, they repel electrons into the Si bulk. In other words, clusters introduce an electric field at the junction leading to carrier re-distribution in the underlying substrate, similar to that at heterojunctions (Capasso and Margaritondo 1987) and metal–oxide–semiconductor interfaces (Sze 1981, p 380). Therefore, charge-transfer interaction becomes visible in I–V characteristics.

We compared tunnelling currents obtained for different cluster types and densities to assess cluster charging. Effective cluster-induced charge at the surface is presented in figure 6 as a function of exposure dose for Si_6H_x and $AsSi_2H_x$ clusters. As reverse current is proportional to electron density at the Si surface (see the appendix), we calculated the effective charge as $(I_{cl} - I_{ox})/I_{ox}$, where the reverse current in the cluster-deposited area (I_{cl}) and that on the oxide (I_{ox}) were taken at a reverse bias of -3 V. The negative value means reduced electron density at the Si surface due to the surface dipole, i.e. the cluster charges negatively (acceptor-like behaviour). The effective charge increased gradually with the number of clusters, providing evidence for charge trapping at the clusters. We obtained -0.8 electron for C_{60}, which is in accordance with the electron-attracting nature of the cluster reported in the literature (Dresselhaus *et al* 1996, Suto *et al* 1997). This value represents a relative strength for cluster coupling, and the strongest coupling was observed for Si clusters containing an arsenic atom that kept one extra electron at the vacant orbital.

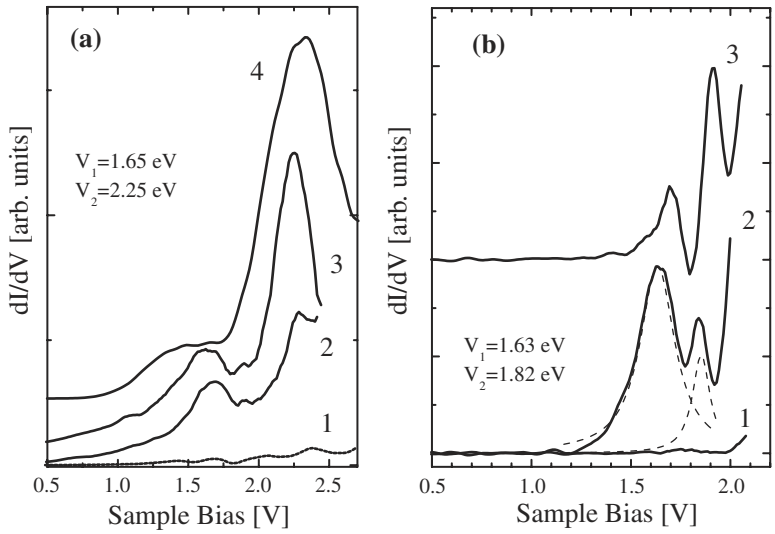

Figure 7. Conductance ($\mathrm{d}I/\mathrm{d}V$) spectra of C_{60} (a) and Si_6H_x (b) clusters on oxidized Si(100) (boron, $\sim 4 \times 10^{15}$ cm^{-3}) at onset conductances of 0.3 (2), 0.7 (3) and 2.0 nS (4) in (a), and 0.15 (2) and 0.3 nS (3) in (b). Curve 1 was obtained on surface prior to cluster deposition. Dashed curves in (b) are Lorentzian fits of curve 2. Curves 3–4 in (a) and the curve 3 in (b) have been shifted for sake of clarity.

4. Resonance electron injection at forward bias

4.1. Resonant tunnelling spectra

The fact that the forward current features were different for C_{60} and Si_6H_x clusters indicates their cluster-related origins. We focused on the conductance spectra of clusters at a moderate injection rate, whereas, as mentioned above, Si_6H_x clusters exhibited the possibility of migration and different current behaviour (see figure 4) at high injection rates. Figure 7 shows ($\mathrm{d}I/\mathrm{d}V$) spectra calculated from I–V characteristics averaged over dozens of clusters. The spectra were obtained at different onset conductances, i.e. different vacuum gap widths. We fitted the conductance peaks by Lorentzian functions to obtain peak positions and dispersions. Cluster-related peaks are clearly seen at 1.6 ± 0.2 and 1.8 ± 0.15 V for Si_6H_x and at 1.6 ± 0.4 and 2.3 ± 0.3 V for C_{60}, while no appreciable structure is observed for oxidized surfaces. We did not see any reproducible structures below 1 V for either cluster, indicating that there were no cluster-related states near the Fermi level. The energy separation between experimentally observed resonances is comparable to the LUMO–LUMO + 1 gap obtained for C_{60} at the Si(111)-(7 × 7) surface and at metal surfaces (Dresselhaus *et al* 1996, Lu *et al* 2003). We note that Hersam *et al* (2000) reported a similar LUMO-derived ($\mathrm{d}I/\mathrm{d}V$) peak at ∼1.6 eV when C_{60} was attached to individual dangling bonds on a hydrogenated Si(100) surface (boron doped, 0.1 Ω cm).

We observed a small (<0.05 eV) upward shift in Si_6H_x peaks and in the dominant C_{60} resonance with onset conductance increase from 0.3 to 2 nS. With conductance increase (vacuum gap decreases), a larger part of the applied voltage drops on the oxide spacer lifting the orbital energy with respect to the silicon Fermi energy. However, the oxide barrier is narrow compared to the vacuum gap, and this geometrical asymmetry prevents considerable voltage drop on the oxide spacer as well as the occurrence of SET effects. This is in contrast

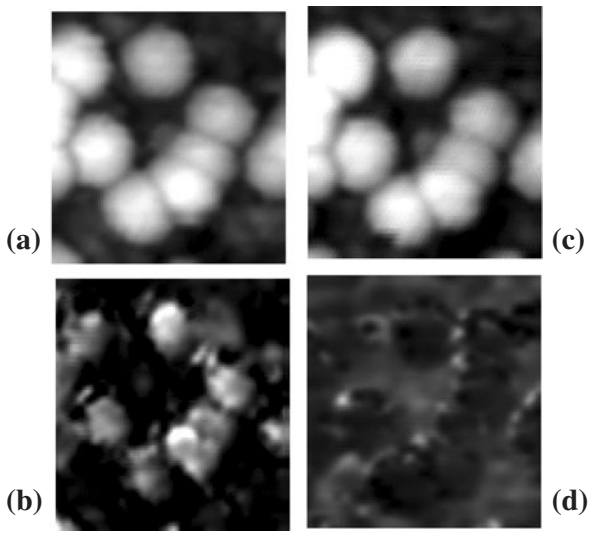

Figure 8. STM topographs ((a) and (c)) and (dI/dV) maps ((b) and (d)) of C_{60} obtained simultaneously from the same 7.5 × 7.5 nm^2 area at onset voltages of 2.3 V ((a) and (b)) and of 2.7 V ((c) and (d)). Brighter contrast in (b) corresponds to conductance resonance at ∼2.3 V in figure 7(a). The grey scale is 1.2 nm in ((a) and (c)) and 3.5 V in ((b) and (d)). Inhomogeneous distribution within C_{60} is seen in (b).

to the case reported by Porath and Millo that in their C_{60}/metal junctions about 2/9 of the total applied voltage dropped on the large barrier between C_{60} and the metal surface formed with hydrocarbons resulting in SET effects (Porath and Millo 1997).

4.2. Resonant tunnelling maps of C_{60}

To confirm the origin of conductance peaks we measured (dI/dV) signal distribution along the surface. Figure 8 has STM topographs and (dI/dV) maps obtained at two onset voltages corresponding to on-resonance and off-resonance electron injection for the C_{60} deposited surface. While the STM topographs were acquired at a constant current of 1.9 nA, (dI/dV) maps were obtained by superimposing a small ac voltage (10 mV_{pp}, 30 kHz) on the onset voltage, and current response was measured with a lock-in amplifier at every point of the STM image. When constant-current conditions are maintained by total current through all states available for tunnelling, the (dI/dV) signal represents a fraction of available states near the onset voltage, thus tracking the resonance energy of clusters. The (dI/dV) signal was ∼3 times larger on the cluster position and localized within ∼1 nm for resonance injection at 2.3 V, while few variations occurred for off-resonance injection at 2.7 V. The apparent height of C_{60} changed with forward bias from ∼1.0 nm (at 1.5–2.8 V) to ∼1.4 nm (at 1.2 V), while it decreased dramatically below 1.2 V, again indicating that resonant tunnelling by the C_{60} orbital contributed to total tunnelling current above 1.2 V.

The C_{60} resonance at 2.3 V demonstrates the spatial inhomogeneity within a cluster together with intensity variations from cluster to cluster. While a homogeneous distribution is seen for the cluster at the top centre of figure 8(b), clusters in the bottom right corner have from two to four intensity variations. Inhomogeneous intensity derives from the fact that the orbital is not isotropic for free C_{60}, which produces spatial intensity variations that depend on cluster orientation with respect to the substrate. When C_{60} is rotated, it produces spatial averaging

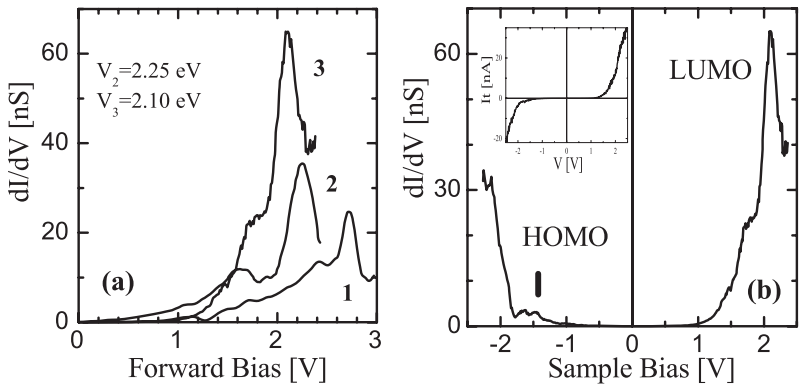

Figure 9. (a) Conductance spectra of C_{60} at oxidized Si(100) substrate with dopant densities of $\sim 8 \times 10^{14}$ cm^{-3} (curve 1), $\sim 4 \times 10^{15}$ cm^{-3} (curve 2) and $\sim 3 \times 10^{18}$ cm^{-3} (curve 3). Observed resonance shift is $\sim$0.15 V for curves 2 and 3. Two peaks are seen in curve 1 at 2.45 ± 0.90 eV (Lorentzian width) and 2.70 ± 0.15 eV. (b) Wide-range conductance spectrum of C_{60} at high-doped Si substrate (boron, $\sim 3 \times 10^{18}$ cm^{-3}) and corresponding current–voltage characteristic (inset) were obtained at an onset voltage of +2 V and $G_o = 5$ nS. Resonance conductance of the C_{60} HOMO at -1.5 V is about one order lower than that of the LUMO.

resulting in homogeneous intensity in the $(\mathrm{d}I/\mathrm{d}V)$ maps. Investigation of $\sim$60 clusters revealed that the abundance of rotating clusters was $\sim$40%. In fact, the internal structure of C_{60} was observed when the cluster rotation was frozen at 7 K on metal (Gaisch *et al* 1993, 1994, Behler *et al* 1993, Sakurai *et al* 1996, Lu *et al* 2003) or immobilized on Si(111)-(7×7) surfaces (Wang *et al* 1992, Hou *et al* 1999, Hersam *et al* 2000). Lu *et al* demonstrated energy-resolved spectral $(\mathrm{d}I/\mathrm{d}V)$ maps of C_{60} on Ag(100) where each orbital had peculiar distributions within C_{60}. For example, the LUMO + 1 was localized at the pentagonal rings, while the $(\mathrm{d}I/\mathrm{d}V)$ map of the LUMO had inverted contrast. Our conductance mapping confirmed the correspondence of observed resonance to the unoccupied orbital of C_{60}, and the conductance spectra in figure 7(a) represent the orientation-averaged orbital conductance of C_{60}.

For a heavily doped Si(100) substrate a broad HOMO-derived resonance appeared at $\sim$1.5 eV, although its magnitude was about an order smaller than the LUMO resonance (figure 9(b)). At forward bias, the Fermi energy of the probe followed the applied voltage, similar to the metal substrate case. At reverse bias, however, a significant fraction of the applied voltage dropped on the depletion region, and the conditions creating the resonance conductance through the HOMO may occur at very high voltages for low-doped substrates. In contrast, the fraction is small for high-doped substrates because of the narrower depletion region, and HOMO resonance becomes accessible at relatively low voltages. A similar energy for the HOMO resonance was obtained for antimony- (Sb-) doped Si substrates with a dopant density of $\sim 4 \times 10^{18}$ cm^{-3}. The derived LUMO–HOMO gap was less than 3 eV for a dopant density of $\sim 3 \times 10^{18}$ cm^{-3}.

5. Cluster orbital alignment

In the previous section, we assigned the features in conductance spectra (figure 7) to resonance-like transitions involving the LUMO and LUMO + 1 of the clusters. Resonance effects in tunnelling spectroscopy were discussed by Persson and Baratoff (1987). They envisaged a resonant scattering process where the tunnelling electron creates a virtually charged molecule that then rapidly re-emits the electron into the vacant states of the adjacent metal. The process

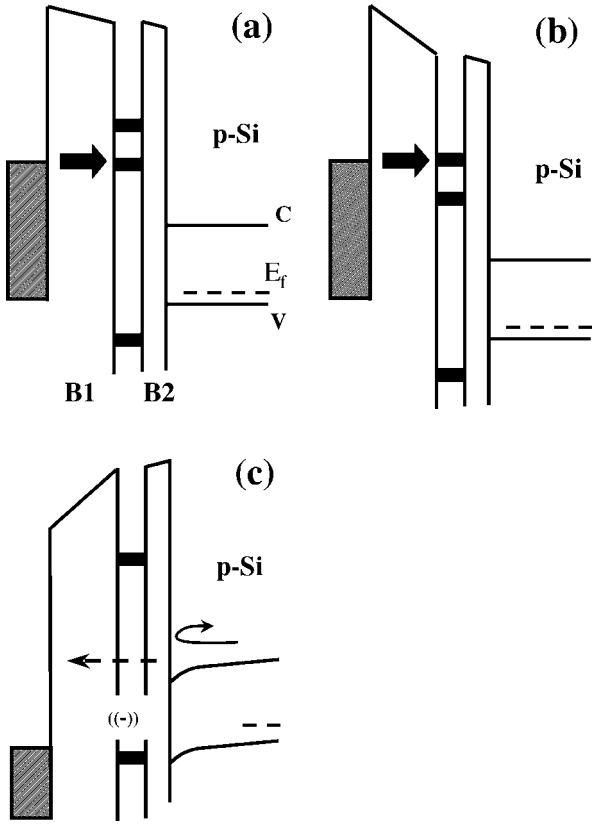

Figure 10. Energy diagrams of STM junction at oxidized Si(100) surface containing cluster resonances. ((a) and (b)) Resonant electron injection conditions through LUMO and LUMO + 1 at V_1 and V_2 bias voltages, respectively. (c) Alignment of $AsSi_2H_x$ orbital that leads to current blocking at reverse bias by trapped negative charge.

is resonance-like in that conductance enhancement is greatest when applied bias places the energy of the source electrode (the STM probe in our case) near the energy of the vacant orbital of the molecule. This indicates that the LUMO for C_{60} and Si_6H_x clusters is located above the conduction band minimum (CBM) of the Si crystal as we did not see any resonance tunnelling below 1 V, i.e., within the Si forbidden gap, and their effective charge was less than 1 electron. This is depicted in figure 10 where at sample bias V_1 tunnelling electrons are injected into the LUMO of an atomic cluster, while at bias V_2 the LUMO + 1 comes to play. Accordingly, we place the LUMO of C_{60} about ∼1.6 eV above the silicon Fermi energy, i.e., approximately 0.7 eV above the CBM for low dopant density, while the LUMO + 1 lies about 1.4 eV above the CBM. The HOMO of C_{60} is ∼1.5 eV below the silicon Fermi energy. Similarly, the LUMO of Si_6H_x clusters is about ∼0.7 eV above the CBM, while the HOMO is placed 0.3–0.5 eV below the valence band maximum according to the LUMO–HOMO gap of 2.1–2.3 eV obtained on the Si(111)-(7 × 7) surfaces (Uchida *et al* 2003b). In contrast, when the half-occupied orbital of $AsSi_2H_x$ clusters is located below the silicon Fermi level (figure 10(c)), it traps an electron and blocks electron tunnelling at reverse bias (see figure 5).

We noted that the resonance energy of the C_{60} LUMO + 1 shifted when a substrate with a higher dopant density was used (figure 9(a)). The threefold degenerate LUMO + 1 t_{1g} originates

in states with an angular momentum of $l = 6$, and it was shifted downward, while the t_{1u} LUMO derived from $l = 5$ became broader and overlaid the higher-energy orbital. The LUMO + 1 shift of ∼0.15 eV for curves 2 and 3 is comparable to the Fermi energy difference for these substrates (∼0.17 eV).

One may conceive that the electron affinity is one of the factors determining the line-up of the cluster orbital to the substrate similar to semiconductor heterostructures. However, in contrast to bulk materials a small cluster can accept a limited number of electrons due to the small density of vacant orbital levels and less stability in charged states. Moreover, electrostatic surface dipole and structural distortion in the charged state lift off degeneracy of the orbital, which causes complex changes in the electronic spectrum of clusters due to shifting and splitting of the cluster orbital. While the origin of resonance shift is still being investigated, the fact that energy shift in the C_{60} orbital was observed for a number of substrates with different dopant densities suggests that the orbital energy of C_{60} aligns with respect to the silicon conduction band edge and, consequently, reflects Fermi energy shift.

The large width of resonance tunnelling bands here is due to several factors. While thermal broadening of the tunnelling probability is ∼120 meV (∼5 kT) (Persson and Baratoff 1987), the distribution of cluster–silicon distance due to thickness variation of the oxide spacer increases inhomogeneous broadening of resonances. Furthermore, the junction field and cluster bonding to surface atoms cause orbital splitting, producing additional broadening. As tunnelling spectroscopy is not limited by selection rules as optical spectroscopy is, variations in orbital splitting create a spectrum broadening.

Electronic coupling is also an essential factor influencing the excited state lifetime and resonance width (Gadzuk 1970, Gata and Antoniewicz 1993). Sufficient overlap of the cluster orbital and the Si band states shortens the lifetime of the excited state and broadens resonance. The overlap between C_{60} and a conductive substrate has previously been discussed within the context of the distance dependence of optical excitation dipole damping (Kuhnke *et al* 1997) and electron-stimulated fragmentation of C_{60} (Bolotov and Kanayama 2003), where excitation decay time increased with the cube of the cluster–substrate distance. Therefore, a narrower conductance resonance can be obtained for a thicker spacer. We actually observed peak width variation from 0.15 to 0.90 eV in figures 7(a) and 9(a), but at present we cannot correlate it with the spacer thickness.

6. Conclusion

An ADBT junction, which was formed with an STM metal probe separated by a vacuum barrier from the cluster layer assembled on the oxidized Si(100) substrate, demonstrated diode-like behaviour. We separately investigated both the cluster-related conductance and cluster-induced surface dipole for C_{60}, Si_6H_x ($x \leqslant 7$) and $AsSi_2H_x$ clusters at submonolayer coverage. For electron extraction from the p-type Si substrate, we found reduction in the junction current with an increase in the cluster density as a result of the cluster-induced surface dipole where negative charge at the clusters partially blocked the junction current for low-doped Si substrates. We evaluated effective cluster-induced charge at the Si surface, which depended on cluster structure and composition.

For electron injection from the STM probe, conductance spectra of the junction showed cluster-specific enhancement originating in resonance-like electron tunnelling through the molecular orbital of the clusters. The enhancement was spatially localized within a ∼1 nm diameter and distributed within the C_{60} cage. We found that the resonant-tunnelling energy of LUMO, LUMO + 1 and HOMO shifted with the doping levels of the substrate, suggesting the possibility of measuring the silicon Fermi energy. Oscillations in current–voltage dependence

at high electron injection were tentatively ascribed to SET effects in Si_6H_x clusters at a distance from the surface where they appeared larger in height. Our results demonstrate that STM operation in an ADBT junction configuration is particularly informative in an analysis of cluster-related conductance and cluster coupling to semiconductor surfaces.

Acknowledgments

The authors would sincerely like to thank Dr Takehide Miyazaki of the National Institute for Advanced Industrial Science and Technology (AIST), Dr Hidefumi Hiura of NEC Corp. (Japan) and Dr. Tetsuya Tada of the ASRC-AIST for their invaluable discussions. This work was supported in part by the New Energy and Industrial Technology Development Organization (NEDO) of Japan.

Appendix

A.1. Cluster-induced surface dipole

The current–voltage relationship of a metal–insulator–semiconductor junction (Green *et al* 1974) can be expressed as

$$I_{\text{tun}} = A f_{\text{tun}}(d, \phi_t) J_{\text{o}} \left[\exp \frac{qV}{kT} - 1 \right],$$

where V is the applied voltage, f_{tun} is the tunnelling probability as a function of width d and energy height ϕ_t of the insulator barrier and A is the contact area. At $V > 0$, forward bias conditions, the current grows exponentially, while $I_{\text{tun}} \sim J_{\text{o}}$ at reverse bias. J_{o} is the reverse saturation current density, given by

$$J_{\text{o}} = J_{\text{dif}} + J_{\text{rg}},$$

where the diffusion part is

$$J_{\text{dif}} = \frac{q D_n n_{\text{i}}^2}{L_n N_{\text{a}}}$$

and the generation–recombination part is

$$J_{\text{rg}} \sim \frac{n_{\text{i}} W}{\tau_{\text{e}}}.$$

Here, N_{a} is the dopant density, τ_{e} is the effective lifetime, n_{i} is the intrinsic free carrier density and W is the width of the semiconductor depletion region. The diffusion coefficient D_n and the Debye length L_n correspond to electrons in p-Si. Under dark conditions and low density of Si gap states $J_{\text{dif}} > J_{\text{rg}}$. When tunnelling probability f_{tun}, D_n and L_n are constant, the junction current is proportional to the density of minority carriers (electrons) $n = n_{\text{i}}^2 / N_{\text{a}}$ at the Si surface, i.e. $I_{\text{tun}} \sim n$.

We calculated the effective cluster-induced change at the surface as

$$Q = \frac{I_{\text{cl}} - I_{\text{ox}}}{I_{\text{ox}}} \simeq \frac{n_{\text{cl}}}{n},$$

where I_{cl} and I_{ox} are the reverse currents on the cluster deposited area and on the initial oxide. n_{cl} is the difference in the surface electron density due to the clusters.

The assumption of constant tunnelling probability is valid for small As-doped clusters (figure 5), and is partially true for C_{60}. While the large C_{60} size changed the junction barrier, the junction width was always adjusted to maintain constant tunnelling probability with and

without clusters at forward bias. It maintained f_{tun} constant, no matter whether the width d or the effective barrier height ϕ_t changed. Change in reverse current, therefore, is caused by the cluster-induced surface dipole through charge re-distribution at the Si surface.

References

Amlani I, Rawlett A M, Nagahara L A and Tsui K 2002 *Appl. Phys. Lett.* **80** 2761
Aviram A and Ratner M A 1974 *Chem. Phys. Lett.* **29** 277
Behler S, Lang H P, Pan S H, Thommen-Geiser V and Güntherodt S 1993 *Z. Phys.* B **91** 1
Bitzer T, Rada T, Richardson N V, Dittrich T and Koch F 2000 *Appl. Phys. Lett.* **77** 3779
Bolotov L and Kanayama T 2002 *Appl. Phys. Lett.* **81** 1684
Bolotov L and Kanayama T 2003 *Phys. Rev.* B **68** 033404
Bolotov L N, Makarenko I V, Shulekin A F and Titkov A N 1995 *Surf. Sci.* **331–333** 468
Bredimas V 1994 *J. Appl. Phys.* **75** 7922
Bumm L A, Arnold J J, Dunbar T D, Allara D L and Weiss P S 1999 *J. Phys. Chem.* **103** 8122
Capasso F and Margaritondo G 1987 *Heterojunction Band Discontinuities: Physics and Device Applications* (Amsterdam: North-Holland)
Chen J, Wang W, Reed M A, Rawlett A M, Price D W and Tour J M 2000 *Appl. Phys Lett.* **77** 1224
Donhauser Z J, Mantooth B A, Kelly K F, Bumm L A, Monnell J D, Stapleton J J, Price D W Jr, Rawlett A M, Allara D L, Tour J M and Weiss P S 2001 *Science* **292** 2303
Dresselhaus M S, Dresselhaus G and Eklund P C 1996 *Science of Fullerenes and Carbon Nanotubes* (New York: Academic)
Dujardin G, Walkup R E and Avouris Ph 1992 *Science* **268** 1590
Gadzuk J W 1970 *Phys. Rev.* B **1** 2110
Gaisch R, Berndt R, Gimzewski J K, Reihl B, Schlittler R R, Schneider W-D and Tschudy M 1993 *Appl. Phys.* A **57** 207
Gaisch R, Berndt R, Schneider W-D, Gimzewski J K, Reihl B, Schlittler R R and Tschudy M 1994 *J Vac. Sci. Technol.* B **12** 2153
Gata M A and Antoniewicz P R 1993 *Phys. Rev.* B **47** 13797
Gimzewski J K and Joachim C 1999 *Science* **283** 1683
Green M A, King F D and Shewchun J 1974 *Solid-State Electron.* **17** 551
Feenstra R M, Vaterlaus A, Yu E T, Kirchner P D, Lin C L, Woodall J M and Pettit G D 1993 *Semiconductor Interfaces at the Sub-Nanometer Scale* ed H W M Salemnik and M D Pashley (Dordrecht: Kluwer) p 127
Fujita S, Watanabe H, Maruno S and Ichikawa M 1997 *Appl. Phys. Lett.* **71** 885
Hersam M C, Guisinger N P and Lydin J W 2000 *Nanotechnology* **11** 70
Hiura H, Miyazaki T and Kanayama T 2001 *Phys. Rev. Lett.* **86** 1733
Hou J G, Jinlong Y, Haiqian W, Qunxiang L, Changgan Z, Hai L, Wang B, Chen D M and Quingshi Z 1999 *Phys. Rev. Lett.* **83** 3001
Kaiser W J, Bell L D, Hecht M N and Grunthaner F J 1988 *J. Vac. Sci. Technol.* A **6** 519
Kanayama T 1994 *Japan. J. Appl. Phys.* **33** L1792
Kelly M J 1995 *Low Dimensional Semiconductors* (New York: Oxford University Press)
Kita K, Ihara M, Sakaki K and Yamada K 1997 *J. Appl. Phys.* **81** 6246
Kuhnke K, Becker R, Epple M and Kern K 1997 *Phys. Rev. Lett.* **79** 3246
Li D Q, Bishop A, Gim Y, Shi X B, Fitzsimmons M R and Jia Q X 1998 *Appl. Phys. Lett.* **73** 2645
Liu H C, Buchanan M, Aers G C, Wasilewski Z R, Moore W T, Devine R L S and Landheer D 1991 *Phys. Rev.* B **43** 7086
Lu X, Grobis M, Khoo K H, Louie S G and Crommie M F 2003 *Phys. Rev. Lett.* **90** 096802
Margaritondo G 1999 *Rep. Prog. Phys.* **62** 765
Mazur U and Hipps K W 1994a *J. Phys. Chem.* **98** 8169
Mazur U and Hipps K W 1994b *J. Phys. Chem.* **98** 5824
Miyata N and Ichikawa M 2001 *Japan. J. Appl. Phys.* **40** L1271
Miyata N, Watanabe S and Ichikawa M 1999 *J. Vac. Sci. Technol.* B **17** 978
Miyazaki T, Uda T, Stich I and Tarakura K 1996 *Chem. Phys. Lett.* **261** 346
Ottaviano L, Santucci S, Di Nardo S, Lozzi L, Passacantando M and Picozzi P 1997 *J. Vac. Sci. Technol.* A **15** 1014
Persson B N J and Baratoff A 1987 *Phys. Rev. Lett.* **59** 339
Porath D and Millo O 1997 *J. Appl. Phys.* **81** 2241
Qiu X H, Nazin G V and Ho W 2003 *Science* **299** 542

Reed M A, Zhou C, Muller C J, Burgin T P and Tour J M 1997 *Science* **278** 252
Roland C, Meunier V, Larade B and Guo H 2002 *Phys. Rev.* B **66** 035332
Sakurai T, Wang X D and Hashizume T 1996 *Mater. Sci. Forum* **232** 119
Saricifici N S, Braun D, Zhang C, Srdanov V I, Heeger A J, Stucky G and Wudl F 1993 *Appl. Phys. Lett.* **62** 585
Shen J, Kramar G, Tehrani S, Goronkin H and Tsui R 1995 *IEEE Electron Device Lett.* **16** 178
Suda Y and Koyama H 2001 *Appl. Phys. Lett.* **79** 2273
Suto S, Sakamoto K, Wakita T, Hu C W and Kasuya A 1997 *Phys. Rev.* B **56** 7439
Sze S M 1981 *Physics of Semiconductor Devices* 2nd edn (New York: Wiley–Interscience)
Tabe M and Tanimoto M 1991 *Appl. Phys. Lett.* **58** 2105
Tans S J, Verschueren A R M and Dekker C 1998 *Nature* **393** 49
Uchida N, Bolotov L and Kanayama T 2003a *Japan. J. Appl. Phys.* 1 **42** 707
Uchida N, Bolotov L and Kanayama T 2003b *Japan. J. Appl. Phys.* 2 **42** 204
Wang X D, Hashizume T, Shinohara H, Saito Y, Nishina Y and Sakurai T 1992 *Japan. J. Appl. Phys.* **31** L983
Wolf E L 1985 *Principles of Electron Tunneling Spectroscopy* (New York: Oxford University Press)
Xue Y and Datta S 1999 *Phys. Rev. Lett.* **83** 4844